scientific reports

Check for updates

OPEN

Autophagy mediates the impact of *Porphyromonas gingivalis* on short-chain fatty acids metabolism in periodontitis-induced gut dysbiosis

Jiahui Sun[1], Xiaoxuan Wang[1,2], Junhong Xiao[1], Qiudong Yang[1], Xin Huang[1,2], Zhengkun Yang[1], Heyu Liu[1], Yuqi Liu[1], Huiyi Wang[1], Zhendong Huang[1], Li Ma[1,2,3]✉ & Zhengguo Cao[1,2,3]✉

***Porphyromonas gingivalis* (*P. gingivalis*), the main pathogen responsible for periodontitis, is linked to systemic disorders via the oral-gut axis. Short-chain fatty acids (SCFAs) are vital for gut health, but their role in *P. gingivalis*-induced gut disorders remains unclear. This study utilized metabolomics and 16 S rRNA sequencing to explore gut microbiota and SCFAs levels in *P. gingivalis*-induced periodontitis mouse models. Significant changes were observed in gut, including a reduction in SCFAs-producing bacteria, such as *Lactobacillus*, *Ligilactobacillus*, *Allobucalum*, and a notable decrease in *Firmicutes* and *Actinobacteriota*. The intestinal permeability tests and histological analyses revealed that periodontitis led to epithelial inflammation, reduced mucin secretion, and compromised gut barrier integrity. In vitro experiments with Caco-2 cells co-cultured with *P. gingivalis* showed that the bacterium disrupted cellular junctions by impairing autophagy, specifically through the ATG5-LC3 pathway, leading to decreased expression of tight junction proteins and reduced SCFA absorption. Remarkably, rapamycin treatment both in vitro and in vivo restored gut barrier function by enhancing autophagy, increasing tight junction protein expression, and promoting SCFAs absorption via MCT1 and SMCT1, alongside GPR43/GPR109a pathway activation. These findings reveal autophagy's novel role in regulating SCFAs metabolism in *P. gingivalis*-induced gut dysbiosis, offering insights for preventing and treating periodontitis-related systemic diseases.**

Keywords *Porphyromonas gingivalis* (*P. gingivalis*), Short-chain fatty acids (SCFAs), Autophagy, Oral-gut axis, 16S rRNA gene sequencing

Periodontitis, the leading cause of tooth loosening and mobility, can result in tooth loss and masticatory dysfunction, affecting both nutrition and aesthetics[1]. It is a prevalent chronic inflammatory disease, chiefly initiated by dental plaque, with *P. gingivalis* being a major pathogen[2]. Moreover, periodontitis has been associated with systemic inflammatory diseases such as diabetes[3], hyperlipidemia[4], and non-alcoholic fatty liver disease[5] resulting from metabolic dysregulation, along with autoimmune conditions like rheumatoid arthritis[6] and inflammatory bowel disease[7] through the oral-gut axis. The underlying regulatory mechanisms include the direct ingestion of oral pathogens, transmission through the bloodstream, and the migration of immune cells[8,9]. However, the precise processes by which *P. gingivalis* induces gut dysbiosis in periodontitis remain unclear.

It was reported that saliva ingestion introduces 10^12 bacteria every day[10–12]. Specically, 0.6% of the gut microbiota derived from saliva in individuals with periodontal health, while the percentage increased to 5.88% in patients with periodontitis[13]. Changes in the composition and quantity of gut microbiota can affect electrolyte and fluid transport through toxin secretion, leading to intestinal permeability and inflammation[14]. Furthermore, the interplay between gut microbial metabolites and immunity is a crucial mechanism regulating gut homeostasis. SCFAs synthesized through dietary fiber fermentation, including butyrate, acetate, and propionate primarily generated in the colon, are acknowledged as indicators of a healthy gut ecosystem[15], regulating appetite, innate

[1]State Key Laboratory of Oral & Maxillofacial Reconstruction and Regeneration, Key Laboratory of Oral Biomedicine Ministry of Education, Hubei Key Laboratory of Stomatology, School & Hospital of Stomatology, Wuhan University, Wuhan, China. [2]Department of Periodontology, School & Hospital of Stomatology, Wuhan University, Wuhan, China. [3]These authors contributed equally: Li Ma and Zhengguo Cao. ✉email: mali2017@whu.edu.cn; caozhengguo@whu.edu.cn

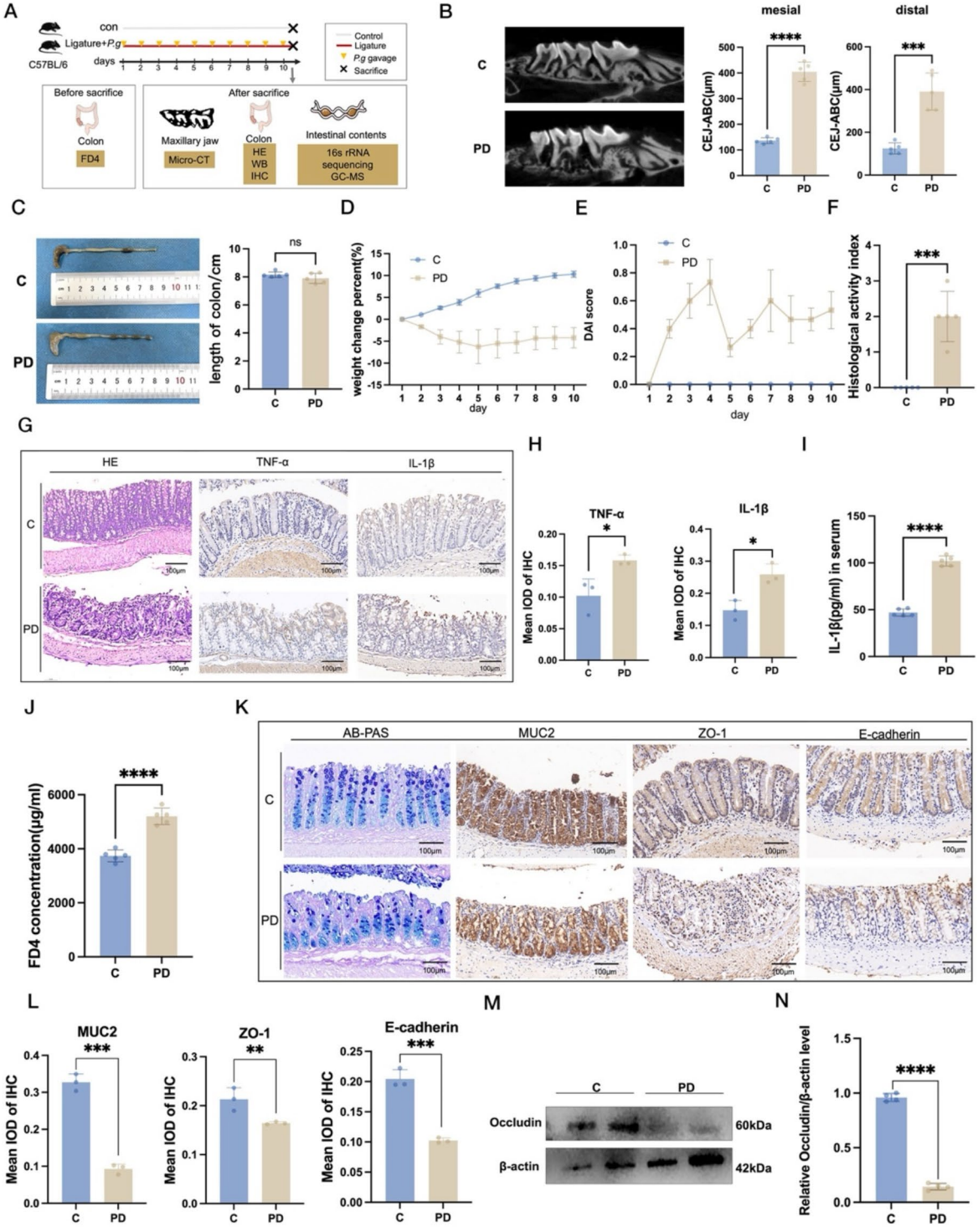

and adaptive immunity[16]. Some bacterial species belonging to the *phyla Firmicutes* and *Bacteroidetes* are capable of producing SCFAs efficiently. Specifically, butyric acid, serves as a crucial energy source for intestinal epithelial cells and preserves the integrity of the gastrointestinal barrier by regulating mucin production and tight junction expression[17]. During periodontitis, *P. gingivalis* has been reported contribute to various changes in metabolites such as tryptophan metabolism[18], choline metabolism[19], and microbiota-linoleic acid metabolism[20]. However, alterations in SCFAs metabolism and their interaction with *P. gingivalis* in periodontitis-induced gut disorders are poorly understood.

Autophagy, a self-degradation process, is reported to regulate various aspects of gastrointestinal physiology, including epithelial structure, metabolism, inflammatory pathways, and infection defense[21]. Studies have reported that autophagy is involved in ketone metabolism in intestinal epithelial cells by targeting the monocarboxylate transporter MCT1 through the mTORC1-autophagy pathway[22]. Interestingly, MCT1 is a key transporter for

◀**Fig. 1**. Gut dysbiosis induced by *P. gingivalis* infection in periodontitis. (**A**) Design of the animal experiments ($n = 5$/group). (**B**) Micro-CT analysis of alveolar bone loss (left) and distance between cemento-enamel junction (CEJ) and alveolar bone crest (ABC) (right). (**C**) Colon morphology and length (**D**) Body weight change percentage. (**E**) Disease activity index (DAI). (**F**) Histological activity index of colon. (**G**) Representative images of H&E and immunohistochemistry staining of TNF-α and IL-1β in colonic tissue. Scale bar, 100 μm. (**H**) Integrated mean optical density (IMOD) using ImageJ and quantification of TNF-α and IL-1β. Data are presented as the mean ± SD from 3 randomly selected fields per sample. (**I**) ELISA test of IL-1β concentration in serum. (**J**) Quantification of serum fluorescein isothiocyanate (FITC)-dextran (4 kDa). (**K**) Representative images of AB-PAS and immunohistochemical staining of MUC-2, ZO-1 and E-cadherin in colon. Scale bar, 100 μm. (**L**) Integrated mean optical density (IMOD) using ImageJ and quantification of MUC-2, ZO-1 and E-cadherin. Data are presented as the mean ± SD from three randomly selected fields per sample. (**M**) Expression of Occludin in colon epithelia cells isolated from mice in two groups. (**N**) Relative quantification of Occludin expression in western blotting. Data represent the mean ± SD from three independent experiments. All the data are presented as mean ± SD (****$P < 0.0001$, ***$P < 0.001$, **$P < 0.01$ and *$P < 0\ 0.05$).

SCFAs absorption and is crucial for their protective effects. However, the role of autophagy in SCFAs metabolism within intestinal epithelial cells and its impact on *P. gingivalis*-induced gut dysbiosis have not yet to be explored.

Our study explored the impact of *P. gingivalis* infection in periodontitis on gut homeostasis through both in vivo and in vitro experiments, focusing on microbiota composition, SCFAs production, and function in mice. Additionally, we provide the first evidence of the interaction between autophagy and SCFAs metabolism in the periodontitis-induced gut microenvironment with *P. gingivalis* infection.

Results

Periodontitis induced gut inflammation and barrier dysfunction in mice

We successfully induced experimental periodontitis in mice via ligature and *P. gingivalis* gavage for 10 days, with increased alveolar bone loss (Fig. 1A,B). Colon length did not significantly differ between groups (Fig. 1C). However, PD mice experienced significant weight loss from the 3rd day of *P. gingivalis* gavage ($p < 0.05$) (Fig. 1D). Post-modeling, PD group feces showed occasional changes like increased stickiness and yellowish discoloration. The DAI score peaked on the 4th day and then gradually increased again (Fig. 1E), while the HAI score was higher in periodontitis-induced mice (Fig. 1F). H&E staining revealed mild to moderate inflammatory cell infiltration and less than 25% crypt shortening in the PD group (Fig. 1G). Inflammatory factors increased in intestinal mucosal mucus and serum of the PD group, with anti-inflammatory factors decreased (Fig. 1G, H, I and S1D). Additionally, periodontitis elevated gut permeability, with decreased ZO-1 and E-cadherin expression (Fig. 1J,K). AB-PAS staining and MUC-2 IHC showed reduced mucin secretion from colonic glands in the periodontitis group (Fig. 1K,L). Occludin, a key tight junction protein, significantly decreased post-periodontitis induction (Fig. 1M and S2). These findings suggest periodontitis may exacerbate gut disorders and inflammation by compromising the intestinal mucosal barrier.

Periodontitis altered gut microbiota composition and reduced healthy bacterial populations in mice

The Venn diagram showed 880 common OTUs between groups and 4048 and 2078 unique OTUs in healthy and periodontitis groups, respectively (Fig. 2A). Microbial structure analysis indicated a strong difference in colon contents between periodontitis and healthy groups (ANOSIM, $R = 0.928$, $p = 0.0111$, Fig. 2B). α-diversity analysis revealed significant microbiota alterations (observed species $p = 0.072$) in periodontitis and control samples. While Chao1 and ACE indicated reduced species richness in the PD group ($p = 0.068$, $p = 0.01$, Fig. 2C), richness and evenness scores showed no significant differences (Shannon $p = 0.504$, Simpson $p = 0.419$). PCoA analysis showed decreased diversity in the PD group (Jaccard $p = 0.01$; weighted unifrac $p = 0.01$, Fig. 2D,E).

The bacteria in colon detected consisted mainly of *Bacteroidetes*, *Firmicutes*, and *Proteobacteria* (Fig. 2F). The *phylum Actinobacteriota* and *Firmicutes* showed a significant tendency to decrease in abundance, and *Bacteroidota* increased in the PD group compared to the C group. Greater changes of microbiota at the genus level were also observed (Fig. 2G), the predominant genera of each group included *Lactobacillus*, *Ligilactobacillus*, *Allobucalum*, *Bacteroides*, *Alloprevotella*, *Alistipes*, and *Helicobecter*, etc. The proportions of *Lactobacillus* and *Ligilactobacillus* were higher in C group. LDA and LEfSe analysis [LDA score (log10 = 4)] was performed on differentially distributed taxa between control and PD group (Fig. 2H,I). Thirty-six taxa were found to be significantly different between the two groups. Specifically, LDA value of *Muribaculaceae* was highest in the PD group while *Lactobacillaceae* had the highest LDA value in the control group. These indicated that periodontitis induced the decrease proportion of healthy condition-associated bacteria.

Immunofluorescence staining revealed *P. gingivalis* clusters in colon tissue of ligature and *P. gingivalis*-gavaged mice (Fig. S1A), indicating potential interaction with intestinal epithelial cells. Krona charts showed increased *Porphyromonas* abundance in the PD group (Fig. S1B).

Periodontitis reduced SCFAs production in colon microenvironment of mice

Short-chain fatty acids (SCFAs) and medium-chain fatty acids (MCFAs) serve as crucial energy sources and signaling molecules, influencing carbohydrate and lipid metabolism and the gut microbiome-immune axis. All eleven major MCFAs and SCFAs were identified except heptanoic acid in the PD group (Fig. 3A). Statistical analysis revealed significant depletion of SCFAs in the PD group, including isovaleric acid ($p < 0.001$), valeric

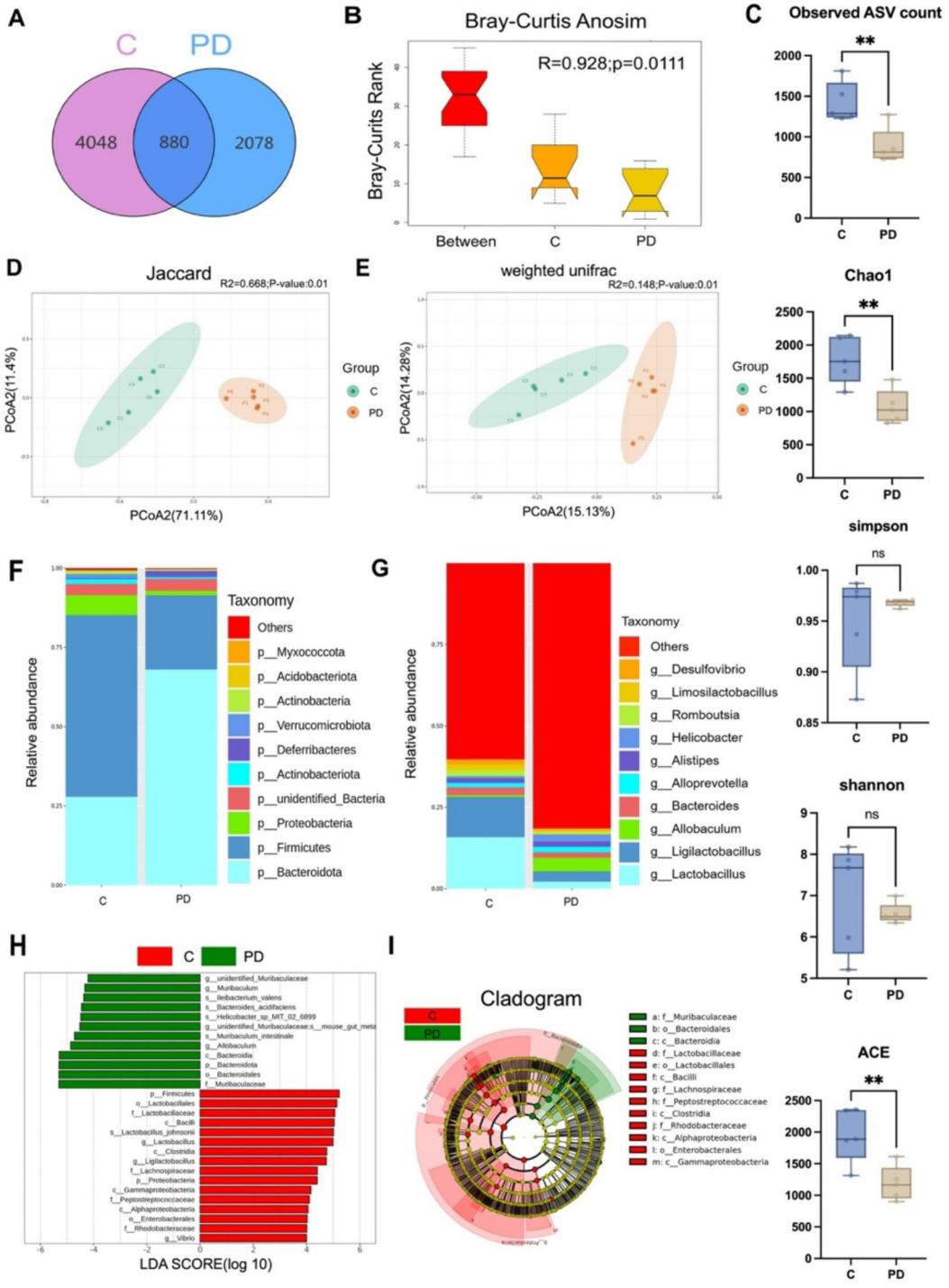

Fig. 2. Alteration of gut microbiota with *P. gingivalis* infection in periodontitis according to the 16 S rRNA data. (**A**) Venn diagram for bacterial operational taxonomic units (OTU) compositions in two groups ($n=5$). (**B**) analyses of similarities (ANOSIM) based on Bray-Curtis distance. (**C**) Alpha diversity of gut microbiota. Observed amplicon sequence variants (ASV) count, species richness (Chao1 and ACE index), species richness and eveness (Shannon and Simpson index). Each box plot represents the median, interquartile range, minimum, and maximum values. (**D**) Jaccard and (**E**) weighted unifrac in Principal coordinate analysis (PCoA) according to Mann-Whitney U-test. (**F**,**G**) LDA Effect Size (LEfSe) Cladograms showing differences in the bacterial taxa between two groups (**H**,**I**) Relative abundance of microbiota at the phylum (left) and genus (right) levels. All the data are presented as mean ± SD (****$P<0.0001$, ***$P<0.001$, **$P<0.01$ and *$P<0$ 0.05).

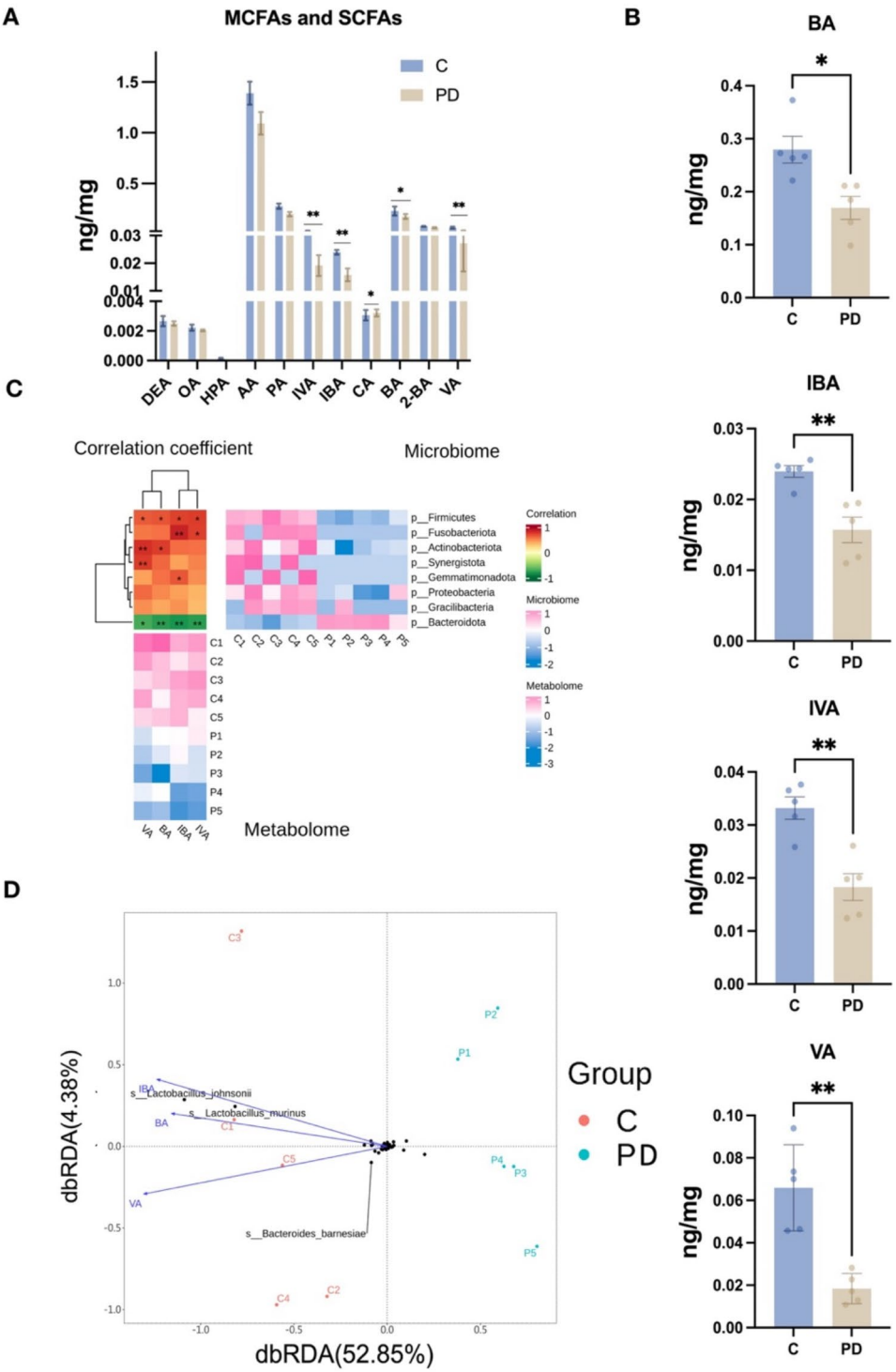

Fig. 3. Changes in SCFAs production in the colon of mice with *P. gingivalis* infection in periodontitis. (**A**,**B**) Concentration of medium-chain and short-chain fatty acids in colon contents. (**C**) The correlation heatmap of microbiota at phylum level and metabolome in colon contents. (**D**) Distance-based redundancy analysis (dbRDA) biplot of colon contents showing the correlation between the microbiota and alteration in SCFAs. *DEA* decanoic acid, *OA* octanoic acid, *HPA* heptanoic acid, *AA* acetic acid, *PA* propionic acid, *IVA* isovaleric acid, *IBA* isobutyric acid, *CA* caproic acid, *BA* butyric acid, *2-BA* 2-methylbutyric acid, *VA* valeric. The length of the vectors indicates the relative importance of the parameter. All the data are presented as mean ± SD (****$P < 0.0001$, ***$P < 0.001$, **$P < 0.01$ and *$P < 0$ 0.05).

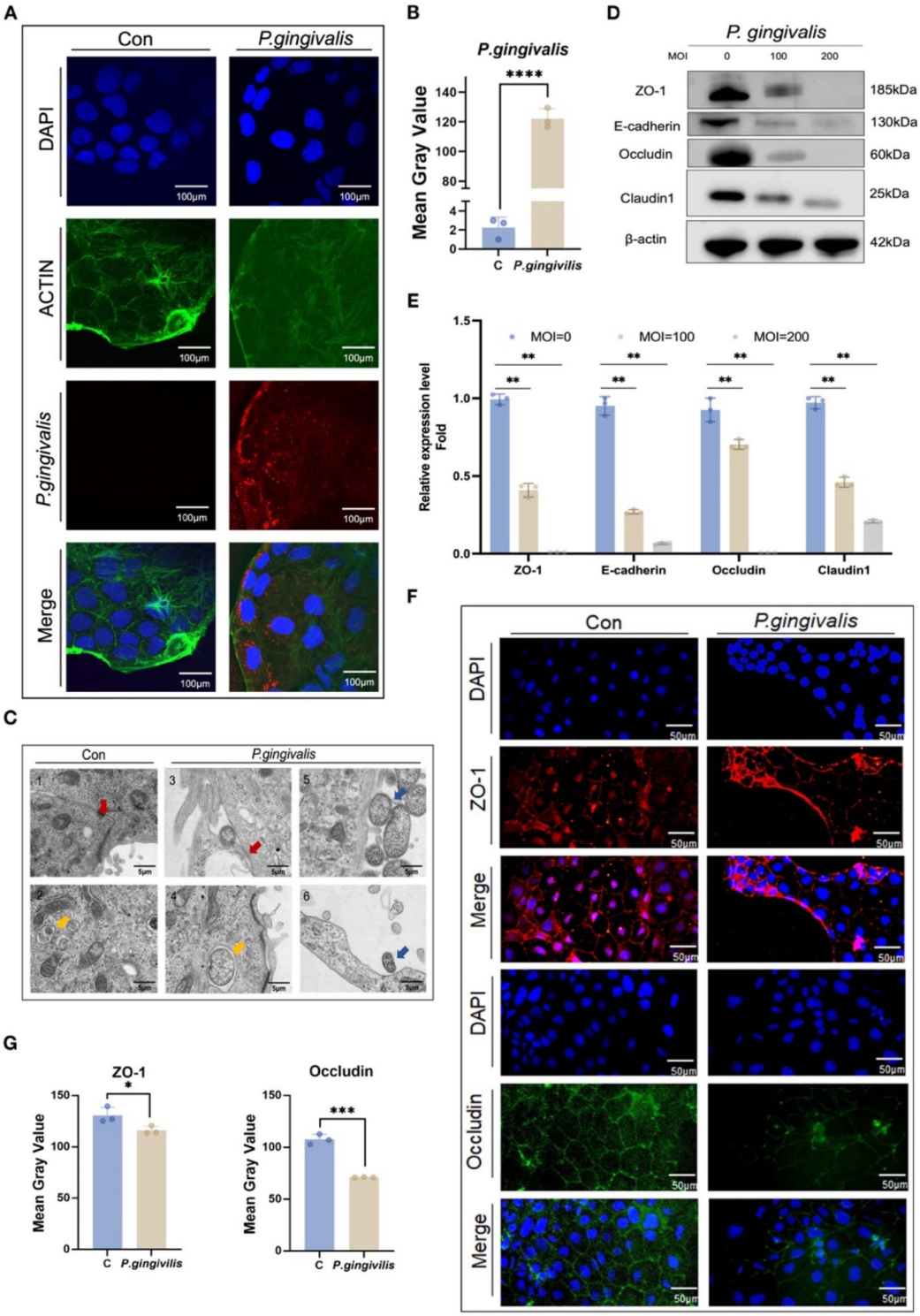

acid ($p < 0.01$), butyrate ($p < 0.05$), and isobutyric acid ($p < 0.01$), with other fatty acids showing decreased levels but no significant differences except for a slight increase in caproic acid (Fig. 3B).

Figure 3C and Fig. S1E lists other typical gut microflora-related metabolites by Pearson's correlation coefficient that are highly correlated with gut. Overall, bacteria like *Firmicutes* and *Actinobacteriota*, major SCFAs producers, decreased significantly in the PD group, while some *Bacteroidota*, also SCFAs producers, increased. Distance-based redundancy analysis showed low collinearity among butyrate, isobutyric acid, and valeric acid, with positive correlations to *Lactobacillus_johnsonii* and *Lactobacillus_murinus* (IBA, r2 = 0.616 $p = 0.032$; VA r2 = 0.581 $p = 0.017$, Fig. 3D). Abundance of SCFAs-producing bacteria like *Lactobacillus* and *Ruminococcaceae* decreased (Fig. S1C).

◀**Fig. 4**. Invasion of *P. gingivalis* facilitated damage of intercellular junction in human intestinal epithelial (Caco-2) cells. (**A**) Confocal images of uptake of *P. gingivalis* by Caco-2 cells. Scale bar: 100 μm. (**B**) Quantitative analysis of *P. gingivalis* expression was performed based on immunofluorescence staining. Images were captured from three biological samples per group, with five randomly selected regions analyzed per sample. (**C**) Transmission electron microscopy (TEM) of *P. gingivalis* invasion in Caco-2 cells: C1. Normal intercellular tight junction between two cells; C2. Vesicles in untreated cell; C3. Loss of integrity of tight junctions in between cells and basolateral entry of *P. gingivalis*; C4. Intracellular *P. gingivalis* was found within vesicular structures with single enclosed membranes; also noticed Caco-2 cells organisms inside the intestinal epithelial cell, without endocytic vacuoles surrounding them; C5-6. *P. gingivalis* fimbriae-mediated adhesion and their interaction with Caco-2 cells. Red arrows showed the tight junctions between two cells. Yellow arrows showed the vesicular structures in cells. Blue arrows showed the intimate interaction between *P. gingivalis* and cells. Scale bars: 5 μm (**D**) Western blot analysis: Decreased expression of ZO-1, E-cadherin, Occludin and Claudin1 in *P. gingivalis* infected cells (MOI = 200). (**E**) Relative quantification of ZO-1, E-cadherin, Occludin and Claudin1 expression in western blotting. (**F**) Immunofluorescence staining of ZO-1 and Occludin: Representative images showing reduced expression of ZO-1 (red, upper panels) and Occludin (green, lower panels) in *P. gingivalis* infected cells. Scale bar: 50 μm. (**G**) Quantitative analysis of ZO-1 and Occludin expression were performed based on immunofluorescence staining. Images were captured from three biological samples per group, with five randomly selected regions analyzed per sample. Statistical analysis confirms significant reduction in ZO-1 and Occludin expression in infected cells.

P. gingivalis infection disrupted intercellular barrier with inhibition of autophagic pathway in Caco-2 cells

Caco-2 cells were cocultured with *P. gingivalis* at 0, 100, 200 MOI for 24 h. Intriguingly, labeled *P. gingivalis* invaded Caco-2 cells (MOI = 200), especially at the cell periphery, around nuclei (Fig. 4A,B). TEM depicted close interaction between *P. gingivalis* and intestinal epithelial cells, with clustered *P. gingivalis* along cell surfaces, interacting with indented surfaces and reducing tight junction density (Fig. 4C). Western blot and IF confirmed *P. gingivalis*-induced degradation of tight junction and adhesion proteins in an MOI-dependent manner (Fig. 4D,E,F,G and S3).

RNA-Seq analysis of *P gingivalis*-infected Caco-2 cells revealed 3318 differentially expressed genes, with fatty acid metabolism and autophagosome assembly enriched in GO analysis (Fig. 5A,B and S4). Although most detected SCFAs showed decreasing trends in infected cells, no statistical differences were observed (Fig. 5C). Downregulation of 27 autophagy-related genes, including MAP1LC3B, was noted in the *P. gingivalis*-infection group (Fig. 5D). *P. gingivalis* significantly impaired the ATG5-LC3 autophagy pathway, potentially leading to Caco-2 dysfunction and damage (Fig. 5E,F,G,H). Interestingly, TEM showed *P. gingivalis* enclosed within a single-membrane vesicle, indicating escape from host immune response. Combined with the downregulation of Bcl2-related apoptosis genes (Fig. S1C), we deduced that *P. gingivalis* may escape host immune response and immune homeostasis disruption.

Autophagy enhanced SCFAs absorption to protect against impaired gut barrier integrity associated with periodontitis

To explore autophagy and SCFAs metabolism regulation in *P. gingivalis*-induced intestinal injury, Caco-2 cells were pre-treated with rapamycin, an autophagy activator, followed by co-culture with *P. gingivalis*. Rapamycin significantly improved barrier indicators, including occludin, ZO-1, E-cadherin, and claudin-1 expressions, and reduced FITC-dextran permeability in transwell plates in infected cells (Fig. 6A–E and S5).

Decreased MCT1 and SMCT1 expression in Caco-2 cells exposed to *P. gingivalis*, indicating impaired SCFAs absorption (Fig. 6A,B,F,G and S6). Rapamycin effectively rescued the expression of these transport proteins and promoted GPR43 and GPR109a activation (Fig. 6F,G and S6). In periodontitis-challenged mice, rapamycin enhanced autophagy, partially restored goblet cells, Muc2 secretion, E-cadherin, and ZO-1 protein expression, and reduced inflammatory cell infiltration in intestinal tissue (Fig. 6H,I, and S1D). These findings suggest that enhanced autophagy strengthens intestinal barrier integrity by restoring SCFAs absorption (Fig. 7).

Discussion

The mouth and gut are two crucial digestive organs, each also serving as a major microbial ecosystem. Oral pathogens like *P. gingivalis* can cause periodontitis and, through the oral-gut axis, disrupt the balance of gut microbiota, which may contribute to various systemic diseases. However, the specific mechanisms by which *P. gingivalis* influences gut dysbiosis are still not fully understood. Our findings revealed significant alterations in gut microbial composition and reduced SCFAs levels in the colons of periodontitis mice, which were linked to gut dysfunction. Additionally, we found that activating autophagy enhanced SCFAs absorption and GPCR signaling in Caco-2 cells, providing evidence for the role of autophagy in regulating SCFAs metabolism during *P. gingivalis* infection.

Literature reports highlight how periodontal pathogen gavage alters the gut microbiome, shedding light on the connection between oral bacterial burden and gut inflammatory diseases[6,20,23,24]. And proactive periodontal treatments have shown promise in improving gut and overall health via the oral-gut axis[25,26]. Our experimental design, incorporating ligation and *P. gingivalis* administration, to better imitate the swallow situation of periodontitis patients. As the duration of ligation and *P. gingivalis* gavage increased, the mice experienced a progressive decline in body weight. Previous studies have reported significant weight loss in both young (4-week-old) and aged (76-week-old) mice following oral administration of *P. gingivalis*[27]. This weight loss was observed

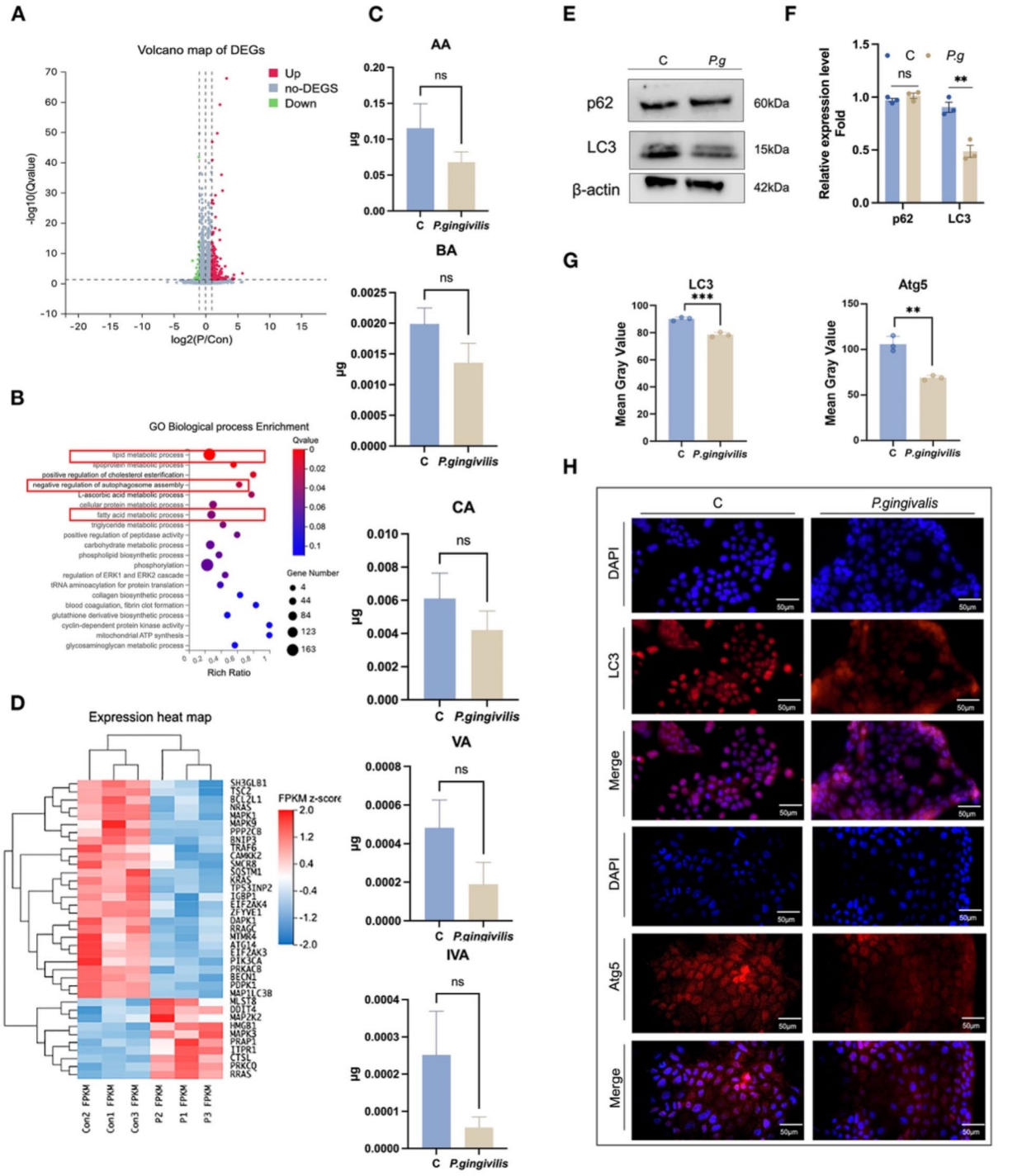

Fig. 5. *P. gingivalis*-disrupted autophagic pathway and short-chain fatty acids in human intestinal epithelial Caco-2 cells. (**A**) Volcano plot of DEGs in *P. gingivalis*-infection and normal samples of Caco-2 cells ($n=3$). (**B**) Gene ontology (GO) biological enrichment analyses ($n=3$). (**C**) Concentration of short-chain fatty acids in Caco-2 cells. (**D**) Heatmap of the autophagy-related mRNA profile of Caco-2 cells from *P. gingivalis*-infection group and controls ($n=3$). (**E**) The expression levels of LC3 and p62 in Caco-2 cells were detected by western blotting (**F**) Relative quantification of LC3 and p62 expression in western blotting. (**G**) Quantitative analysis of LC3 and p62 expression were performed based on immunofluorescence staining. Images were captured from three biological samples per group, with five randomly selected regions analyzed per sample. (**H**) Representative images of LC3 and Atg5 immunostaining. Scale bar: 50 μm.

within the first two weeks, and researchers have attributed it to the systemic circulation of bacterial toxins. Just as weight loss is a crucial indicator of successful modeling in widely used mouse colitis models, it results from extensive damage to the intestinal epithelium caused by dextran sulfate sodium (DSS) administration, simulating increased intestinal permeability. This is subsequently accompanied by dysbiosis in the gut microbiota, leading to immune cell infiltration and inflammatory responses[28]. Notably, periodontitis-induced mice exhibited stool changes indicative of oral health influencing digestive disorders. Consistent with prior studies[19,23], we observed elevated pro-inflammatory cytokines in the gut and circulation, reduced levels of key tight junction and adherin proteins, and decreased mucin2 secretion in epithelial tissues, underscoring the systemic impact of periodontitis on intestinal barrier.

Advances in sequencing technology have revealed abnormal clustering of pathogenic bacteria and changes in resident bacteria in gastrointestinal disorders, emphasizing the critical role of gut microbiota in maintaining gut health and responding to immune stimuli[7]. Patients with periodontitis were reported to exhibit moderate dysbiosis in the intestinal microbiome, characterized by reduced species diversity and *Firmicutes*/*Bacteroidetes* frequency[29]. The increased abundance of *P. gingivalis*, in colorectal mucosa of colorectal cancer patients, further emphasized the direct link between periodontal pathogens and gut microbiota dysregulation[30]. However, current research on the intestinal microbiota of periodontitis mice primarily relies on fecal samples[6,23], failing to accurately represent the microbial composition within the gut and exhibiting certain spatial and temporal variabilities[31]. Therefore, we expanded our study by directly characterizing the metatranscriptomic profile of colon contents. Our findings showed an increased abundance of the *Porphyromonas* genus in the periodontitis group, indicating a shift in microbial communities, which was associated with reduced β-diversity, *Firmicutes*/*Bacteroidetes* ratio, and probiotic decline, contributing to elevated inflammatory responses.

About 95% of SCFAs, produced by gut microbiota in the colon, are rapidly absorbed by colonic epithelial cells and support epithelial integrity[32,33]. SCFAs levels are often assessed directly by measuring their concentrations in gut contents, feces, or indicated indirectly by the abundance of SCFA-producing bacteria. Our study revealed a significant reduction in *Firmicutes* and *Actinobacteriota*, indicating that periodontitis leads to reduced SCFA-producing bacteria. This is consistent with previous research showing lower fecal SCFA levels or reduced abundance of SCFA-producing bacteria in patients with inflammatory bowel disease or ulcerative colitis[33]. Moreover, strategies such as prebiotic supplementation[34]or introducing rare SCFA-producing species[35] have been shown to restore SCFAs levels and provide anti-inflammatory effects. In our periodontitis model, we also observed a significant decrease in *Ruminococcaceae*, the primary butyrate producer[15]. These findings underscore that the decline in SCFA-producing bacterial populations is the main driver of reduced SCFAs production.

The absorption of SCFAs primarily relies on two transporter proteins: MCT1, which facilitates H+-coupled uptake of SCFAs in intestinal epithelial cells, and SMCT1, responsible for Na+-coupled uptake of SCFAs. In cells infected with *P. gingivalis*, we also observed a decrease in the expression of these two transporter proteins, further indicating the compromised protective effect of SCFAs under periodontitis conditions. SCFAs play diverse roles, from modulating histone deacetylases activity to promoting immune homeostasis via G-protein coupled receptors (GPR)[17]. GPR43 activation in T cells enhances IL-10 production[36,37], while reduced SCFAs levels hinder GPR109a activation and tight junction protein expression[38]. Limited evidence exists on SCFAs changes induced by periodontitis and their role in gut homeostasis. Our study confirmed reduced SCFAs in periodontitis mice colon and highlighted the vital role of the SCFA-GPR pathway in regulating immune responses to *P. gingivalis* in Caco-2 cells. These findings underscore the intricate relationship among oral health, gut microbiota, and metabolite profiles.

Additionally, we innovatively uncovered the interactions between autophagy-mTOR pathway and SCFAs metabolism process. Reports suggest that SCFAs are known to modulate the mTOR pathway, enhancing IL-10 production and exerting neuroprotective effects via autophagy activation[39,40]. However, the reciprocal effect of mTOR activation on SCFAs uptake remains unexplored. In our study, autophagy activation was initially discovered to effectively restored intercellular junctions disrupted by enhancing SCFAs transportation through MCT1 and SMCT1 proteins. RNA-seq and TEM also revealed downregulation of autophagy as a potential mechanism for periodontal pathogen evasion. In response to periodontal infections, the changes in autophagy levels vary significantly across diversified cell and pathogen types—some exhibit activation, while others show inhibition. Typically, activated autophagy enhance the bactericidal capacity of host cells and reduce inflammation. For instance, *P. gingivalis* lipopolysaccharides induced autophagy in human gingival fibroblasts, ultimately limiting the secretion of pro-inflammatory cytokines[41]. Similarly, *P. gingivalis* was shown to induce autophagy in human umbilical vein endothelial cells, offering protection against endoplasmic reticulum stress-mediated apoptosis[42]. In contrast, our study observed autophagy inhibition in Caco-2 intestinal epithelial cells following *P. gingivalis* infection. This discrepancy may be attributed to: (1) Different cell types exhibit distinct stress responses to pathogens, especially in non-phagocytic barrier cells like epithelial cells. For example, in intestinal epithelial cells such as Caco-2, after *Fusobacterium nucleatum* infection, it initially induces autophagosome formation, but prolonged stimulation leads to autophagosome maturation suppression, manifested as inhibition of autophagy[43]. (2) Based on the specific characteristics of *P. gingivalis*, this bacterium is rather sticky to evade autophagic degradation by residing within autophagic vesicles, allowing it to survive and even reproduce within host cells. In our study, the presence of single-membrane vacuoles around *P. gingivalis* suggests bacterial escape to avoid clearance, such as *Mycobacterium tuberculosis*[44] and *Shigella flexneri*[45]. This suggests that *P. gingivalis* might enter single-membrane vesicles, preventing autophagosome-lysosome fusion and utilizing autophagosomal components for survival[46,47].

These findings offer valuable insights into the complex interactions between autophagy, SCFAs metabolism, and gut dysbiosis during *P. gingivalis* infection, highlighting potential therapeutic targets for managing periodontitis-related gut disorders. While we've minimized limitations, residual bias remains. In vitro experiments can't fully replicate the interactions between *P. gingivalis* and multiple microbial communities

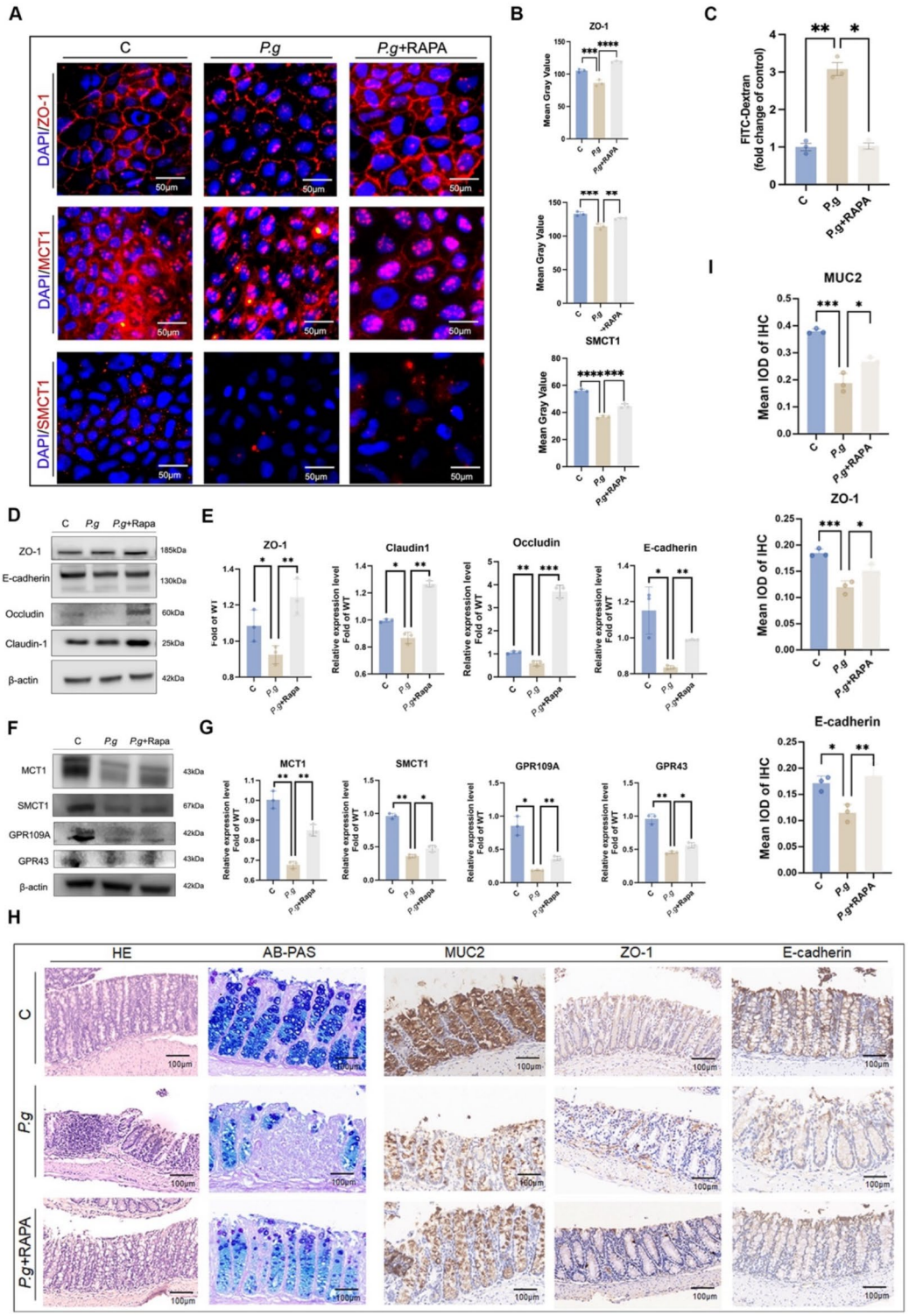

in gut. To further validate the generality of our findings, in vitro models combined with intestinal organoids could be used to pinpoint specific regulatory mechanism in the autophagy pathway and their interaction with downstream SCFAs transport proteins.

In conclusion, *P. gingivalis* infection in periodontitis disrupted gut microbiota composition, reduced SCFAs production, and impaired barrier function. Mechanistically, autophagy was found to regulate SCFAs transport and metabolism via the SMCT1/MCT1-GPCR pathway.

Methods

Bacterial culture and cell culture

P. gingivalis (strain 33277) was cultured anaerobically at 37 °C in trypticase soy broth supplemented with hemin, vitamin K1, and yeast extract. Bacterial density was standardized based on optical density at 600 nm (1

◂**Fig. 6**. Autophagy enhanced SCFAs absorption to safeguard against *P. gingivalis*-induced impairment of gut barrier integrity. (**A**) Representative immunofluorescence photomicrographs of fluorescent localization and expression of ZO-1, MCT1, and SMCT1in Caco-2 cells. Scale bar, 50 μm. (**B**) Quantitative analysis of ZO-1, MCT1, and SMCT1expression were performed based on immunofluorescence staining. Images were captured from three biological samples per group, with five randomly selected regions analyzed per sample. (**C**) Fluorescein isothiocyanate (FITC) dextran (4 kDa) permeability in Caco-2 cells (**D**) Western blot analysis of intercellular junctions (ZO-1, Occludin, E-cadherin, Claudin1) expression in Caco-2 cells. (**E**) Relative quantification of ZO-1, Occludin, E-cadherin, and Claudin1 expression in western blotting. (**F**) Western blot analysis of transporter proteins of SCFAs (MCT1, SMCT1) and G-protein coupled receptors (GPR43, GPR109a) expression in Caco-2 cells. (**G**) Relative quantification of MCT1, SMCT1, GPR43 and GPR109a expression in western blotting. (**H**) Representative images of H&E, AB-PAS and immunohistochemical staining of MUC-2, ZO-1 and E-cadherin. Scale bar, 100 μm. (**I**) Integrated mean optical density (IMOD) using ImageJ and quantification of MUC-2, ZO-1 and E-cadherin. Data are presented as the mean ± SD from three randomly selected fields per sample. All the data are presented as mean ± SD (****$P < 0.0001$, ***$P < 0.001$, **$P < 0.01$ and *$P < 0$ 0.05).

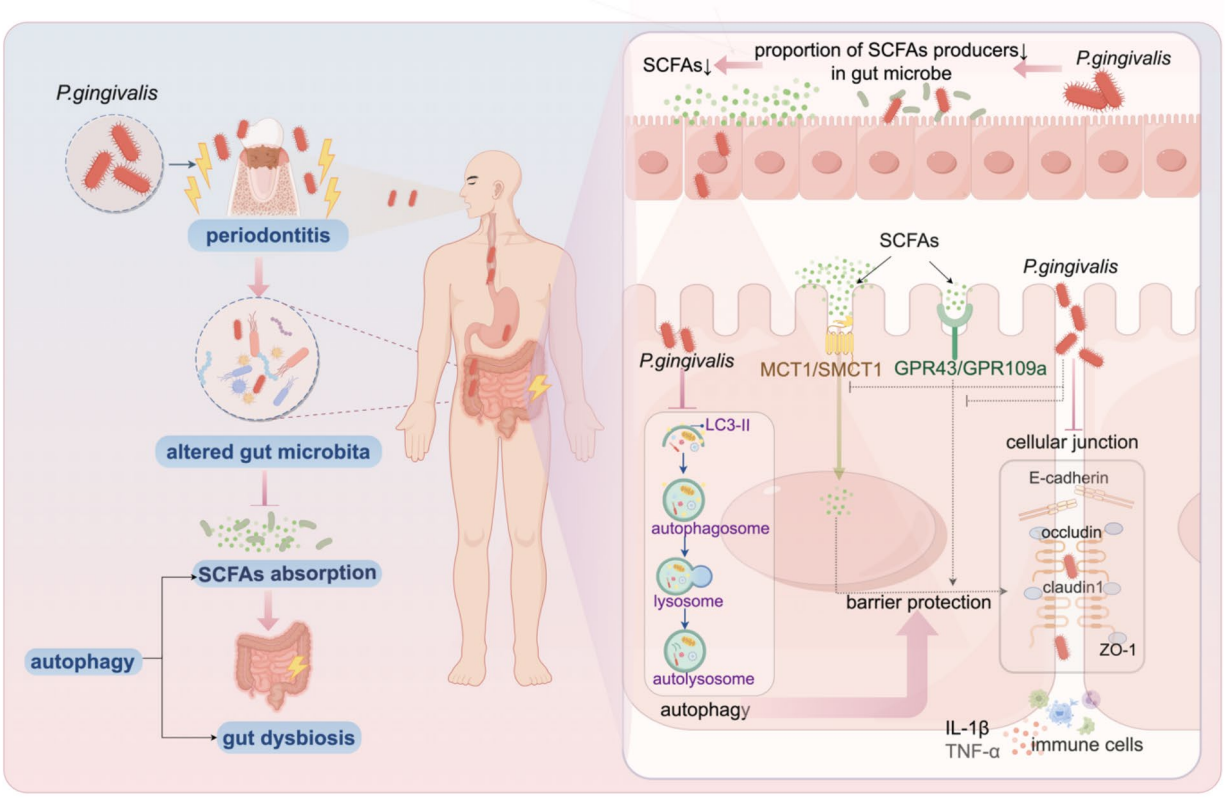

Fig. 7. Scheme depicting of autophagy regulation effect of microbiota SCFAs on *P. gingivalis*-induced gut dysbiosis.

OD = 10^9 *P. gingivalis* /mL) and suspended in 1 ml phosphate-buffered saline (PBS) for oral gavage. Caco-2 cells were cultured in α-MEM supplemented with 20% fetal bovine serum, 1% non-essential amino acids, and 1% penicillin-streptomycin at 37 °C in 5% CO_2 and 95% humidity.

Animal experiments

Animal procedures were conducted in accordance with the Ethics Committee of The Hospital of Stomatology, Wuhan University (S07922090H), adhered to the 8th edition of the Guide for the Care and Use of Laboratory Animals (National Research Council, USA, 2011) and ARRIVE guidelines. Fifteen male C57BL/6J mice (6-week-old, weighing 20–25 g) were housed in a specific pathogen-free environment with standard controlled light and temperature for 1 week before experimentation. Mice were randomly assigned to three groups: C (control, 100uL PBS gavage with no ligature), PD (periodontitis induced by ligature and 100uL *P. gingivalis* gavage), and RAPA (periodontitis plus rapamycin treatment). After acclimation, PD and RAPA mice underwent periodontitis induction by 5 – 0 threads ligature around bilateral maxilla second molars and oral administration

of live *P. gingivalis* for 10 days. RAPA mice received intraperitoneal rapamycin injections (2 mg/kg) on alternate days from the 2nd to the 10th day after ligation.

Body weight and feces were observed daily. On the 10th day, animals were euthanized via CO_2 following eye blood collection. Maxillae and colons were dissected, with colon contents immediately frozen in liquid nitrogen. Colons were fixed in 4% paraformaldehyde for 24 h, then embedded in paraffin. Tissue sections underwent rehydration and were cut into 4 μm slices for histological staining. Isolation of intestinal epithelial cells from the remaining colon was performed as described[48]. Proteins released from lysed cells were clarified by centrifugation, with the resulting supernatant stored on ice for detection.

Micro-computed tomography (Micro-CT)

The fixed maxillae were preserved in 75% alcohol and scanned using a Quantum GX micro-CT scanner (PerkinElmer Inc., Waltham, MA, USA) at 100 kV and 200 μA with a 10 μm resolution. 3D reconstructions of the alveolar bones were generated using NRecon software, and distances between the cementoenamel junction (CEJ) and the alveolar bone crest (ABC) were measured using a data viewer software.

Hematoxylin-eosin (H&E), alcian blue and periodic acid schiff (AB-PAS) stain, and immunohistochemistry

After deparaffinization, tissue sections underwent alcohol gradient and PBS washing. H&E staining followed standard protocols, while colon sections were stained using AB-PAS staining kit (Solarbio.G1285, Solarbio). Immunohistochemical staining was performed using traditional methods described in our previous study[49]. Primary antibodies against the following targets were used: Mucin-2 (ab272692, abcam, 1:2000), ZO-1 (AF5145, affinity, 1:400), E-cadherin (ET1607-75, HUABIO, 1:400), TNF-α (7B8A11, proteintech, 1:400), IL-1β (A16288, Abcolonal, 1:200), IL-10 (8E4b6 proteintech, 1:400). Quantitative analysis of immunohistochemistry staining was performed on three biological samples per experimental group. For each sample, five representative regions were randomly selected for analysis. The intensity of staining was measured using ImageJ software, and the results were averaged to obtain the final values for statistical analysis.

Enzyme-linked immunosorbent assay (ELISA)

Blood samples collected from the intraorbital plexuses of mice were centrifuged at 3,500 × g for 5 min and stored at 4 °C. The supernatant was collected and cryopreserved at −80 °C. IL-1β levels were measured using ELISA detection kits (FANKEW, F2040-B).

Scoring of colon destruction

Histological activity index (HAI) of colonic injury was used as previously described[50]. Briefly, colonic injury was evaluated based on the extent of inflammatory infiltration (0–3), loss of crypt (0–4), and tissue damage. The disease activity index (DAI) was calculated as reported total score [body weight decrease + stool consistency + rectal bleeding] / 3[51]. The scoring criteria were shown as follows: body weight loss (0–4); bloody stools (0–4); diarrhea (0–4). All these evaluations were carried out by the same individual. The o-tolidine method (Yuan Ye, China) was used for qualitative fecal occult blood testing. Fecal samples about the size of mung beans were collected daily at fixed time, using a sterile cotton swab. The sample was placed in a transparent petri dish, avoiding exposure to other liquids or air. Two drops of Solution A (O-tolidine Solution) were added to completely cover the sample, followed by two drops of Solution B (oxidizer). Color changes were observed within two minutes: no color change was labeled with (-); light green turning green was labeled with (+); green turning olive brown (++); blue-brown color darkening to black-brown color (+++); blue-black brown color (++++).

Barrier permeability

For in vivo epithelial permeability assessment, mice received oral administration of FITC-conjugated dextran (60 mg/mL, Sigma-Aldrich). After four hours, serum supernatant was collected and fluorescence intensity measured using the EMax Plus Microplate Reader (excitation: 485 nm, emission: 520 nm). In vitro assessment utilized Transwell Cell Culture plates (Labselect, 0.4 μm) and FITC-conjugated dextran. Caco-2 cells (5 × 10^4 cells per well) were cultured for 14 days in the upper compartments. Following a 24-hour incubation with bacteria (MOI: 200), 5 μL of 10 mg/mL FITC-dextran was added to the upper compartments. After two hours, fluorescence intensity in the lower chamber compartments was quantified.

DNA extraction and 16 S rRNA gene sequencing

Samples were processed as follows: colon contents microbial DNA was extracted using the MagPure Stool DNA KFKit B (Magen, China), then quantified with the Qubit dsDNA BR Assay kit (Invitrogen, USA). Metagenomic analysis of the 16 S rRNA gene was outsourced to Metware Biotechnology Co., Ltd. (Wuhan, China). PCR amplification utilized specific primers (16 S V4: 515 F-806R) and sequencing was performed on the Illumina HiSeq2500 platform. Sequence data underwent processing with Uparse software (v7.0.1001) and taxonomic annotation against a customized SILVA reference database, followed by clustering into Operational Taxonomic Units (OTUs) at 97% similarity. Amplicon Sequence Variants (ASVs) analysis employed Deblur. QIIME assessed alpha and beta diversities, and bacterial abundance was quantified. Principal Coordinate Analysis (PCoA) was performed using R software. Differences between groups were analyzed using Linear Discriminant Analysis Effect Size (LEfSe).

Medium-chain fatty acids (MCFAs) and SCFAs detection

Metware Biotechnology Co., Ltd. (Wuhan, China) conducted the analysis of MCFAs and SCFAs. Samples underwent thawing, homogenization (Ultra Turrax T 25, Sweden), centrifugation, and filtration before GC

analyses. MCFAs and SCFAs, including decanoic, octanoic, heptanoic, acetic, propionic, isobutyric, butyric, isovaleric, valeric, and hexanoic acid, were identified using gas chromatography-tandem mass spectrometry. Chromatographic analysis utilized an Agilent 7890B gas chromatograph system equipped with a DB-5MS column (J&W Scientific, Folsom, CA).

RNA sequencing

Upon reaching 70–80% confluence, Caco-2 cells were exposed to *P. gingivalis* (MOI = 200) for 24 h. Total RNA was extracted using TRIzol reagent (Servicbo). RNA-seq library construction and high-throughput RNA-seq were performed by Wuhan Genomic Institution (BGI HUADA, China) on a BGISEQ-500 sequencer. Gene ontology (GO) pathway analyses were conducted. In the RAPA group, cells were preincubated with rapamycin (200 nm) for 24 h before exposure to *P. gingivalis*.

Transmission electron microscopy (TEM)

Caco-2 cells (5.0 × 10^6 cells/well) were cultured overnight, then co-cultured with *P. gingivalis* (MOI = 200) for 24 h. Samples were fixed in 2.5% glutaraldehyde with 0.1 M sodium cacodylate for 2 h, followed by 1% osmium tetroxide postfixation at 4 °C for 2 h, and ethanol dehydration. After overnight acetone and epoxy resin incubation, solidification occurred at 60 °C for 2 days. Ultrathin slices were obtained using an ultramicrotome (Leica, EM UC7), double-stained with uranyl acetate and lead citrate, then observed under a transmission electron microscope (Tecnai G2 20 TWIN, 200 kV).

Immunofluorescence staining

Samples were infiltrated with 4% paraformaldehyde at room temperature for 20 min. and permeabilized using 0.2% Triton X-100 for 15 min for cells. Subsequently, the cells and tissues were sealed with 5% BSA for 1 h, and then incubated with the primary antibody overnight at 4 °C [*P. gingivalis* (DSHB,61BG1.3, 1:400), ZO-1 (AF5145, affinity, 1:400), Occludin (Santa, sc-133256 1:400), ATG5 (Affinity, AF0155, 1:400), LC3 (Sigma, L7543, 1:400), MCT1(Proteintech, 20139-1-AP, 1:400), SMCT1(Proteintech, NBP1-62527, 1:400)]. Following three washes with PBS, samples were incubated with the secondary antibody at 37 °C for 1 h. Finally, the fluorescence was captured through a fluorescence microscope.

Western blotting

Samples were treated with protease and phosphatase inhibitors, then subjected to SDS-PAGE and transferred to PVDF membranes. After blocking, the membranes were then probed with antibodies: ZO-1 (AF5145, affinity, 1:1000), Occludin (Santa, sc-133256 1:1000), E-cadherin (ET1607-75, HUABIO, 1:5000), claudin1 (Santa, sc-166338, 1:1000), LC3 (Sigma, L7543, 1:1000), p62 (Affinity, AF6456, 1:1000), GPR43(Abclonal, A18592, 1:1000), GPR109a(Abclonal, A15611, 1:1000), MCT1(Proteintech, 20139-1-AP, 1:1000), SMCT1(Proteintech, NBP1-62527, 1:1000) and β-actin(Proteintech, 66009-1-AP, 1:20000). The intensity of the bands was quantified using ImageJ software, and target protein levels were normalized to β-actin. The relative expression levels were calculated as fold changes compared to the control group.

Quantification and statistical analysis

Data were analyzed using GraphPad Prism v.10 Software. Student's t-test and Wilcoxon test compared differences between two groups, while one-way ANOVA assessed differences in three or more groups. A p-value of < 0.05 denoted statistical significance ($^{*}p < 0.05$; $^{**}p < 0.01$; $^{***}p < 0.001$; $^{****}p < 0.0001$), with "ns" indicating non-significant differences.

Data availability

The data analyzed in this study is subject to the following licenses/restrictions: The original contributions presented in the study are included in the article/Supplementary Materials. Further inquiries can be directed to the corresponding authors. Requests to access these datasets should be directed to Zhengguo Cao, caozhengguo@whu.edu.cn.

Received: 20 August 2024; Accepted: 28 October 2024
Published online: 01 November 2024

References

1. Yin, J., Li, Y., Feng, M. & Li, L. <ArticleTitle Language="En">Understanding the feelings and experiences of patients with periodontal disease: a qualitative meta-synthesis. *Health Qual. Life Outcomes.* **20**, 126. https://doi.org/10.1186/s12955-022-02042-5 (2022).
2. Kassebaum, N. J. et al. Global burden of severe periodontitis in 1990–2010: a systematic review and meta-regression. *J. Dent. Res.* **93**, 1045–1053. https://doi.org/10.1177/0022034514552491 (2014).
3. Li, J. et al. Periodontitis in elderly patients with type 2 diabetes mellitus: impact on gut microbiota and systemic inflammation. *Aging (Albany NY).* **12**, 25956–25980. https://doi.org/10.18632/aging.202174 (2020).
4. Huang, Y. et al. Non-surgical periodontal treatment restored the gut microbiota and intestinal barrier in apolipoprotein E(-/-) mice with periodontitis. *Front. Cell. Infect. Microbiol.* **10**, 498. https://doi.org/10.3389/fcimb.2020.00498 (2020).
5. Komazaki, R. et al. Periodontal pathogenic bacteria, Aggregatibacter actinomycetemcomitans affect non-alcoholic fatty liver disease by altering gut microbiota and glucose metabolism. *Sci. Rep.* **7**, 13950. https://doi.org/10.1038/s41598-017-14260-9 (2017).
6. Sato, K. et al. Aggravation of collagen-induced arthritis by orally administered *Porphyromonas gingivalis* through modulation of the gut microbiota and gut immune system. *Sci. Rep.* **7**, 6955. https://doi.org/10.1038/s41598-017-07196-7 (2017).
7. Kitamoto, S. & Kamada, N. Periodontal connection with intestinal inflammation: Microbiological and immunological mechanisms. *Periodontol 2000.* **89**, 142–153. https://doi.org/10.1111/prd.12424 (2022).

8. Pacheco-Yanes, J., Reynolds, E., Li, J. & Mariño, E. Microbiome-targeted interventions for the control of oral-gut dysbiosis and chronic systemic inflammation. *Trends Mol. Med.* **29**, 912–925. https://doi.org/10.1016/j.molmed.2023.08.006 (2023).
9. Yamazaki, K. Oral-gut axis as a novel biological mechanism linking periodontal disease and systemic diseases: A review. *Jpn. Dent. Sci. Rev.* **59**, 273–280. https://doi.org/10.1016/j.jdsr.2023.08.003 (2023).
10. Humphrey, S. P. & Williamson, R. T. A review of saliva: normal composition, flow, and function. *J. Prosthet. Dent.* **85**, 162–169. https://doi.org/10.1067/mpr.2001.113778 (2001).
11. Saygun, I. et al. Salivary infectious agents and periodontal disease status. *J. Periodontal. Res.* **46**, 235–239. https://doi.org/10.1111/j.1600-0765.2010.01335.x (2011).
12. Schmidt, T. S. et al. Extensive transmission of microbes along the gastrointestinal tract. *Elife.* **8** https://doi.org/10.7554/eLife.42693 (2019).
13. Bao, J. et al. Periodontitis may induce gut microbiota dysbiosis via salivary microbiota. *Int. J. Oral Sci.* **14**, 32. https://doi.org/10.1038/s41368-022-00183-3 (2022).
14. Barbara, G. et al. Inflammatory and microbiota-related regulation of the intestinal epithelial barrier. *Front. Nutr.* **8**, 718356. https://doi.org/10.3389/fnut.2021.718356 (2021).
15. Fusco, W. et al. Short-chain fatty-acid-producing bacteria: Key components of the human gut microbiota. *Nutrients.* **15** https://doi.org/10.3390/nu15092211 (2023).
16. Schlatterer, K., Peschel, A. & Kretschmer, D. Short-chain fatty acid and FFAR2 activation - A new option for treating infections? *Front. Cell. Infect. Microbiol.* **11**, 785833. https://doi.org/10.3389/fcimb.2021.785833 (2021).
17. Singh, V. et al. Butyrate producers, The sentinel of gut: Their intestinal significance with and beyond butyrate, and prospective use as microbial therapeutics. *Front. Microbiol.* **13**, 1103836. https://doi.org/10.3389/fmicb.2022.1103836 (2022).
18. Niu, C. et al. Intestinal translocation of live porphyromonas gingivalis drives insulin resistance.*J. Dent. Res.* **103**, 197–207. https://doi.org/10.1177/00220345231214195 (2024).
19. Dong, Z., Lv, W., Zhang, C. & Chen, S. Correlation analysis of gut microbiota and serum metabolome with porphyromonas gingivalis-induced metabolic disorders.*Front. Cell. Infect. Microbiol.* **12**, 858902. https://doi.org/10.3389/fcimb.2022.858902 (2022).
20. Jia, L. et al. Porphyromonas gingivalis aggravates colitis via a gut microbiota-linoleic acid metabolism-Th17/Treg cell balance axis. *Nat. Commun.* **15**, 1617. https://doi.org/10.1038/s41467-024-45473-y (2024).
21. Foerster, E. G. et al. How autophagy controls the intestinal epithelial barrier. *Autophagy.* **18**, 86–103. https://doi.org/10.1080/15548627.2021.1909406 (2022).
22. Uebanso, T. et al. SLC16a6, mTORC1, and autophagy regulate ketone body excretion in the intestinal cells. *Biology (Basel).* 12 https://doi.org/10.3390/biology12121467 (2023).
23. Nakajima, M. et al. Oral Administration of *P. gingivalis* induces dysbiosis of gut microbiota and impaired barrier function leading to dissemination of enterobacteria to the liver. *PLoS ONE.* **10**, e0134234. https://doi.org/10.1371/journal.pone.0134234 (2015).
24. Elzayat, H., Mesto, G. & Al-Marzooq, F. Unraveling the impact of gut and oral microbiome on gut health in inflammatory bowel diseases. *Nutrients.* **15** https://doi.org/10.3390/nu15153377 (2023).
25. de Oliveira, A. M., Lourenço, T. G. B. & Colombo, A. P. V. Impact of systemic probiotics as adjuncts to subgingival instrumentation on the oral-gut microbiota associated with periodontitis: A randomized controlled clinical trial. *J. Periodontol.* **93**, 31–44. https://doi.org/10.1002/jper.21-0078 (2022).
26. Bajaj, J. S. et al. Periodontal therapy favorably modulates the oral-gut-hepatic axis in cirrhosis. *Am. J. Physiol. Gastrointest. Liver Physiol.* **315**, G824–g837. https://doi.org/10.1152/ajpgi.00230.2018 (2018).
27. Giri, S. et al. The effect of Porphyromonas gingivalis on the gut microbiome of mice in relation to aging. *J. Periodontal. Res.* **57**, 1256–1266. https://doi.org/10.1111/jre.13062 (2022).
28. Cochran, K. E., Lamson, N. G. & Whitehead, K. A. Expanding the utility of the dextran sulfate sodium (DSS) mouse model to induce a clinically relevant loss of intestinal barrier function. *PeerJ.* **8**, e8681. https://doi.org/10.7717/peerj.8681 (2020).
29. Baima, G. et al. Effect of periodontitis and periodontal therapy on oral and gut microbiota. *J. Dent. Res.* **220345231222800** https://doi.org/10.1177/00220345231222800 (2024).
30. Wang, X. et al. *Porphyromonas gingivalis* promotes colorectal carcinoma by activating the hematopoietic NLRP3 inflammasome. *Cancer Res.* **81**, 2745–2759. https://doi.org/10.1158/0008-5472.Can-20-3827 (2021).
31. Shalon, D. et al. Profiling the human intestinal environment under physiological conditions. *Nature.* **617**, 581–591. https://doi.org/10.1038/s41586-023-05989-7 (2023).
32. Wang, R. X., Henen, M. A., Lee, J. S., Vögeli, B. & Colgan, S. P. Microbiota-derived butyrate is an endogenous HIF prolyl hydroxylase inhibitor. *Gut Microbes.* **13**, 1938380. https://doi.org/10.1080/19490976.2021.1938380 (2021).
33. Kelly, C. J. et al. Crosstalk between microbiota-derived short-chain fatty acids and intestinal epithelial HIF augments tissue barrier function. *Cell. Host Microbe.* **17**, 662–671. https://doi.org/10.1016/j.chom.2015.03.005 (2015).
34. Kim, S. et al. Hybrid nutraceutical of 2-ketoglutaric acid in improving inflammatory bowel disease: Role of prebiotics and TAK1 inhibitor. *Biomed. Pharmacother.* **171**, 116126. https://doi.org/10.1016/j.biopha.2024.116126 (2024).
35. Ambat, A. et al. Enhancing recovery from gut microbiome dysbiosis and alleviating DSS-induced colitis in mice with a consortium of rare short-chain fatty acid-producing bacteria. *Gut Microbes.* **16**, 2382324. https://doi.org/10.1080/19490976.2024.2382324 (2024).
36. Sun, M., Wu, W., Liu, Z. & Cong, Y. Microbiota metabolite short chain fatty acids, GPCR, and inflammatory bowel diseases. *J. Gastroenterol.* **52**, 1–8. https://doi.org/10.1007/s00535-016-1242-9 (2017).
37. Sun, M. et al. Microbiota-derived short-chain fatty acids promote Th1 cell IL-10 production to maintain intestinal homeostasis. *Nat. Commun.* **9**, 3555. https://doi.org/10.1038/s41467-018-05901-2 (2018).
38. Feng, W. et al. Sodium butyrate attenuates diarrhea in weaned piglets and promotes tight junction protein expression in colon in a GPR109A-dependent manner. *Cell. Physiol. Biochem.* **47**, 1617–1629. https://doi.org/10.1159/000490981 (2018).
39. Park, J. et al. Short-chain fatty acids induce both effector and regulatory T cells by suppression of histone deacetylases and regulation of the mTOR-S6K pathway. *Mucosal Immunol.* **8**, 80–93. https://doi.org/10.1038/mi.2014.44 (2015).
40. Wen, J. et al. Sodium butyrate exerts a neuroprotective effect in rats with acute carbon monoxide poisoning by activating autophagy through the mTOR signaling pathway. *Sci. Rep.* **14**, 4610. https://doi.org/10.1038/s41598-024-55198-z (2024).
41. Bullon, P. et al. Autophagy in periodontitis patients and gingival fibroblasts: unraveling the link between chronic diseases and inflammation. *BMC Med.* **10**, 122. https://doi.org/10.1186/1741-7015-10-122 (2012).
42. Hirasawa, M. & Kurita-Ochiai, T. Porphyromonas gingivalis induces apoptosis and autophagy via ER stress in human umbilical vein endothelial cells. *Mediat. Inflamm.* **2018** (1967506). https://doi.org/10.1155/2018/1967506 (2018).
43. Tang, B. et al. Fusobacterium nucleatum-induced impairment of autophagic flux enhances the expression of proinflammatory cytokines via ROS in Caco-2 Cells. *PLoS ONE.* **11**, e0165701. https://doi.org/10.1371/journal.pone.0165701 (2016).
44. Sturgill-Koszycki, S. et al. Lack of acidification in Mycobacterium phagosomes produced by exclusion of the vesicular proton-ATPase. *Science.* **263**, 678–681. https://doi.org/10.1126/science.8303277 (1994).
45. Ogawa, M. et al. Escape of intracellular Shigella from autophagy. *Science.* **307**, 727–731. https://doi.org/10.1126/science.1106036 (2005).
46. Lee, K., Roberts, J. S., Choi, C. H., Atanasova, K. R. & Yilmaz, Ö. *Porphyromonas gingivalis* traffics into endoplasmic reticulum-rich-autophagosomes for successful survival in human gingival epithelial cells. *Virulence.* **9**, 845–859. https://doi.org/10.1080/21505594.2018.1454171 (2018).

47. Bélanger, M., Rodrigues, P. H. & Dunn, W. A. Jr. Progulske-Fox, A. Autophagy: a highway for *Porphyromonas gingivalis* in endothelial cells. *Autophagy.* **2**, 165–170. https://doi.org/10.4161/auto.2828 (2006).
48. Tsuzuno, T. et al. Ingestion of *Porphyromonas gingivalis* exacerbates colitis via intestinal epithelial barrier disruption in mice. *J. Periodontal Res.* **56**, 275–288. https://doi.org/10.1111/jre.12816 (2021).
49. Xiao, J. et al. CKIP-1 promotes *P. gingivalis*-induced inflammation of periodontal soft tissues by inhibiting autophagy. *Inflammation.* **46**, 1997-2010. https://doi.org/10.1007/s10753-023-01856-9 (2023).
50. Zhang, C. et al. ADP/P2Y(1) aggravates inflammatory bowel disease through ERK5-mediated NLRP3 inflammasome activation. *Mucosal Immunol.* **13**, 931-945. https://doi.org/10.1038/s41385-020-0307-5 (2020).
51. Chen, G. et al. Sodium butyrate inhibits inflammation and maintains epithelium barrier integrity in a TNBS-induced inflammatory bowel disease mice model. *EBioMedicine.* **30**, 317-325. https://doi.org/10.1016/j.ebiom.2018.03.030 (2018).

Acknowledgements
We are extremely grateful to Professor Qingtao Meng from Wuhan University Renmin Hospital for the kind donation of the Caco-2 cell line.

Author contributions
JS: Conceptualization, Methodology, Data curation, Investigation, Methodology, Writing – original draft. XW: Data curation, Funding acquisition. JX: Investigation, Methodology. QY: Formal Analysis, Methodology, Software. XH: Investigation, Funding acquisition. ZY: Investigation, Methodology. HL: Methodology, Validation. YL: Methodology, Software. HW: Investigation, Methodology. ZH: Visualization, Writing – review & editing. LM: Conceptualization, Project administration, Funding acquisition, Supervision. ZC: Funding acquisition, Supervision, Writing – review & editing, Project administration.

Declarations

Competing interests
The authors declare no competing interests.

Ethics declarations
All animal procedures were performed with the approval of the Ethics Committee of The Hospital of Stomatology, Wuhan University (S07922090H), and complied with the ethical standards and guidelines in the 8th edition of the Guide for the Care and Use of Laboratory Animals (National Research Council, USA, 2011). Additionally, we confirmed the study is reported in accordance with ARRIVE guidelines.

Additional information
Supplementary Information The online version contains supplementary material available at https://doi.org/10.1038/s41598-024-77909-2.

Correspondence and requests for materials should be addressed to L.M. or Z.C.